Enhanced Electrochemical Performance of Hybrid Solid Polymer Electrolytes Encompassing Viologen for All-Solid-State Lithium Polymer Batteries

ACS MATERIALS Au
AN OPEN ACCESS JOURNAL OF THE AMERICAN CHEMICAL SOCIETY

pubs.acs.org/materialsau

Article

Enhanced Electrochemical Performance of Hybrid Solid Polymer Electrolytes Encompassing Viologen for All-Solid-State Lithium Polymer Batteries

Natarajan Angulakhsmi, Bebin Ambrose, Swamickan Sathya, Murugavel Kathiresan, Gabriele Lingua, Stefania Ferrari, Erathimmanna Bhoje Gowd, Wenyang Wang, Cai Shen, Giuseppe Antonio Elia, Claudio Gerbaldi,* and Arul Manuel Stephan*

Cite This: https://doi.org/10.1021/acsmaterialsau.3c00010

Read Online

ACCESS | Metrics & More | Article Recommendations | Supporting Information

ABSTRACT: Hybrid solid polymer electrolytes (HSPE) comprising poly(ethylene oxide) (PEO), LiTFSI, barium titanate ($BaTiO_3$), and viologen are prepared by a facile hot press. The physical properties of the HSPE membranes are studied by using small-angle and wide-angle X-ray scattering, thermogravimetric analysis, differential scanning calorimetry, and tensile strength. The prepared hybrid solid polymer electrolytes are also investigated by means of ionic conductivity and transport number measurements. The employed analyses collectively reveal that each additive in the PEO host contributes to a specific property: LiTFSI is essential in providing ionic species, while $BaTiO_3$ and viologen enhance the thermal stability, ionic conductivity, and transport number. The enhanced value in the Li^+-transport number of HSPE are presumably attributed to the electrostatic attraction of TFSI anions and the positive charges of viologen. Synergistically, the added $BaTiO_3$ and viologen improve the electrochemical properties of HSPE for the applications in all-solid-state-lithium polymer batteries.

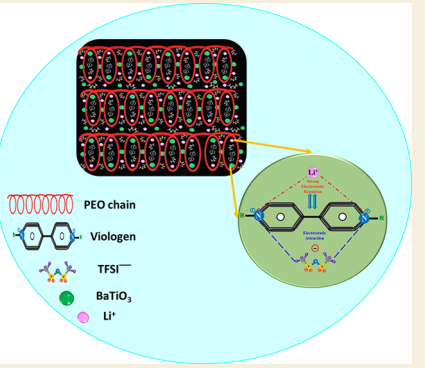

KEYWORDS: *Li metal battery, polymer electrolyte, poly(ethylene oxide), viologen, transport number*

1. INTRODUCTION

The commercialization of lithium-ion batteries (LIBs) has attained the maximum success to power portable electronic devices.[1,2] While LIBs seem to be adequately efficient for mobile phones and laptop computers, they still lack in terms of energy density, power, and safety for the applications in hybrid and plug-in electric vehicles. The state-of-the-art LIB employs organic (nonaqueous) liquid electrolytes which are reactive, flammable, and could combust and eventually cause an explosion of the device in case of overheating during the operation, so that safety still remains as a major concern.[3,4] Long cycling and durability could also be worsened by some parasitic side reactions and leakage of the electrolyte, which are other highly possible events when organic liquids are used. Recently, lithium metal batteries (LMBs) have been at the center of extensive research as next-generation energy storage devices; however, the porous polymeric separators, which are widely employed in LIBs, cannot prevent the growth of lithium dendrites at the anode surface while cycling.[5,6] Among all strategies to eliminate flammability and lithium dendrites, replacing the organic liquid electrolyte with solid electrolytes (SEs) is considered one of the most promising also to contain costs, adding flexibility and opening up to original designs for extending the application range (wearables, health monitoring, etc.).[7] SEs are generally classified as ceramic and polymeric electrolytes, which have been extensively studied for more than three decades. Although fast Li^+-ion ceramic conductors have a transport number (t_{Li+}) close to unity and high thermal stability, they are usually brittle and can hardly provide an efficient ionic interface with the electrodes.[8] On the other hand, polymer electrolytes with good mechanical stability can effectively mitigate the negative effects of dendrites because the physical penetration or rupture caused by mossy dendrites is less probable. Additionally, the flexible nature of the Li^+-ion conductive solid polymers can offer a very good ionic interface between the electrode and the electrolyte.[9]

Despite several advantages, the use of truly solid polymer electrolytes comprising a polymeric host and lithium salt is still hampered by intrinsically low ionic conductivity (10^{-7}–10^{-8} S cm^{-1} at ambient temperature).[10] Among various polymeric hosts, starting from the seminal work of Fenton et al. that practically marked the birth of the field of polymer electrolytes,[11] poly-(ethylene oxide) (PEO) has been widely explored

Received: February 13, 2023
Revised: June 21, 2023
Accepted: June 21, 2023

also to design hybrid electrolytes owing to its appealing properties such as the ability to dissolve salts, affordable price, mechanical strength, and anti-corrosive nature.[10] The conductivity in PEO strongly depends on the segmental motion of the polymer backbone and in turn on the fraction of the amorphous phase. Increasing the amorphous fraction can help in maximizing the mobile phase for ion conduction, but, in doing so, the mechanical strength can be compromised. Composite polymer electrolytes CPEs represent one of the most widely used types of hybrid electrolytes in which a small amount (few percentages) of fine ceramic particles is homogenously dispersed in a polymer−salt complex. Generally, the incorporation of inert ceramic oxides as filler in a polymeric host reduces its crystallinity, facilitates the ionic conduction, and helps preserving the mechanical properties and shear modulus, fundamental to mitigate lithium dendrite formation. The most studied fillers have been nanometric oxides such as SiO_2,[12,13] ZrO_2,[14] Al_2O_3,[15,16] and TiO_2.[17] Also, the ferroelectric $BaTiO_3$ was found to significantly enhance the ionic conductivity[18] depending on the grain size and crystal structure.[19] Indeed, the electrostatic and covalent incorporation of redox molecules have also been investigated to improve the storage capacity and ion transport. Among these, viologen has been identified as a unique molecule with redox mediating properties.[22−24] Very recently, the applications of viologens in energy storage devices have been extensively reviewed.[25]

In order to maximize the mobile phase for ionic conduction improvement, the general view for PEO-based SPEs is to suppress crystallinity by introducing substances that can have a plasticizing effect. Pragmatic approaches to this aim have been indeed the development of hybrid electrolytes also including combinations of more than two lithium-ion conducting phases, such as ionic liquids and deep eutectic solvents,[20] obtaining a sort of hybrid quasi-solid electrolyte (QSE), or liquid electrolytes to obtain gel electrolytes.[21] In the present study, hybrid solid polymer electrolytes (HSPE) comprising various concentrations of PEO, LiTFSI, $BaTiO_3$, and viologen have been prepared by a facile hot-press. LiTFSI (lithium bis(trifluoromethanesulfonyl)imide) has a relevant role as salt in the field of polymer-based electrolytes due to its low dissociation energy and because of charge delocalization that makes ($TFSI^-$) a weakly coordinating anion, so that the Li^+−anion interactions are reduced. Moreover, LiTFSI possesses good ionic conductivity, increased thermal and electrochemical stabilities, lower sensitivity toward moisture than $LiPF_6$, and it creates a stable passivation layer when in contact with metallic lithium.[26] The physical and electrochemical properties of the polymeric separators are systematically analyzed and discussed depending on the Li salt concentration. The cycling tests carried out in an all-solid-state Li/HSPE/$LiFePO_4$ cell revealed the good characteristics of the hybrid electrolyte encompassing the propionic acid viologen, which would contribute to the production of safer lithium-ion cells.

2. EXPERIMENTAL SECTION

2.1. Membrane Preparation

The viologen 1,1′-bis(2 carboxyethyl)-4,4′-bipyridine-1,1′ dibromide (Scheme 1) was synthesized as described in the Supporting Information (see Figure SI 1a−c for NMR characterization).

The HSPEs comprising PEO (mol wt 3×10^5 g mol^{-1}), $BaTiO_3$ (BTO, Alfa Aesar, 99.99% particle size approximately 6 nm), viologen, and the lithium bis(trifluoromethanesulfonyl)-imide (LiTFSI, Aldrich, USA 99.99%) salt were fabricated according to the here-reported procedure. Appropriate ratios of PEO and LiTFSI (Table 1) were carefully dissolved in anhydrous acetonitrile and allowed to stir for 6 h. Then, $BaTiO_3$ was dispersed in the solution, which was then cast and hot pressed to obtain a polymeric membrane 50 to 60 μm thick. The HSPE was stored in a glove box under an Ar atmosphere (H_2O < 1 ppm).

Scheme 1. Structural Formula of the Viologen 1,1′-Bis(2-carboxyethyl)-4,4′-bipyridine-1,1′-dibromide

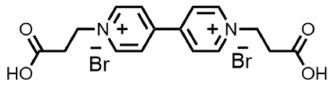

Table 1. HSPE Composition: PEO, BTO, Viologen and LiTFSI Wt%. Degree of Crystallinity (DoC), Lithium Transport Number and Conductivity at 25 °C

sample	PEO	BTO	Viologen	LiTFSI	DoC (%) (±1)	t+	σ (S cm^{-1})
S1	95			5	73	0.16	9.3×10^{-8}
S2	90		5	5	71	0.17	2.8×10^{-5}
S3	90	5		5	64	0.19	2.2×10^{-5}
S4	85	5	5	5	63	0.23	1.3×10^{-4}
S5	70	10	5	15	52		5.1×10^{-5}

2.2. Materials Characterization

2.2.1. Structural and Thermal Characterization. The thermal stability of pure PEO and the HSPEs were determined by thermogravimetric analysis (Netzsch, Germany) in a N_2 atmosphere between ambient temperature and 600 °C at a ramp rate of 10 °C min^{-1}. Differential scanning calorimetry (DSC, Metttler Toledo, USA) was carried out between −100 and 100 °C, at a ramp rate of 10 °C min^{-1}, and the second heating scan was considered to study the crystallization behavior of the membranes.

Wide-angle and small-angle X-ray scattering measurements (WAXS/SAXS) were performed using a XEUSS 2.0 SAXS/WAXS system by Xenocs. The Cu Kα radiation (wavelength = 1.54 Å) was used for data collection in the transmission mode. The two-dimensional X-ray patterns were recorded using an image plate system (Mar 345 detector) and processed using the Fit2D software. Silicon powder and silver behenate were used as standards to calibrate the sample to detector distance for WAXS and SAXS, respectively. The background subtraction was performed on the SAXS data.

Scanning electron microscopy (SEM) images were collected by using a ZEISS Supra 55 VP microscope coupled with the energy dispersive X-ray analysis (EDX) detector for microanalysis. The EDX results for a preliminary characterization of the membranes' composition are presented in Figure SI 2.

X-ray photoelectron spectroscopy (XPS, Thermo Scientific, USA) was performed utilizing Al Kα radiation (photon energy = 1486.7 eV) on the lithium surface with a micro focused monochromator. The lithium metal was collected from a symmetric Li/HSPE/Li cell stored at 60 °C in an Ar filled glovebox and then was placed in an airtight vessel to be transferred to the XPS sample chamber. The data were acquired using Thermo Advantage V5.9925 software and were further analyzed with CASA. The C−C bond obtained at 284.2202 eV (Figure 5) has been considered as a reference for further plotting. The curves were fitted using 90% of Gaussian and 10% of Lorentzian Voigt peak shapes.[28] An electron flood gun was used to neutralize the charge.[29]

The atomic force microscope (AFM, Dimension icon, Bruker) experiment was performed in a glovebox at room temperature. Young's modulus was measured by the PeakForce QNM (Quantitative NanoMechanics) technique. Bruker AFM probe RTESPA-300 with a spring constant of 40 N/m was used for

https://doi.org/10.1021/acsmaterialsau.3c00010
ACS Mater. Au XXXX, XXX, XXX−XXX

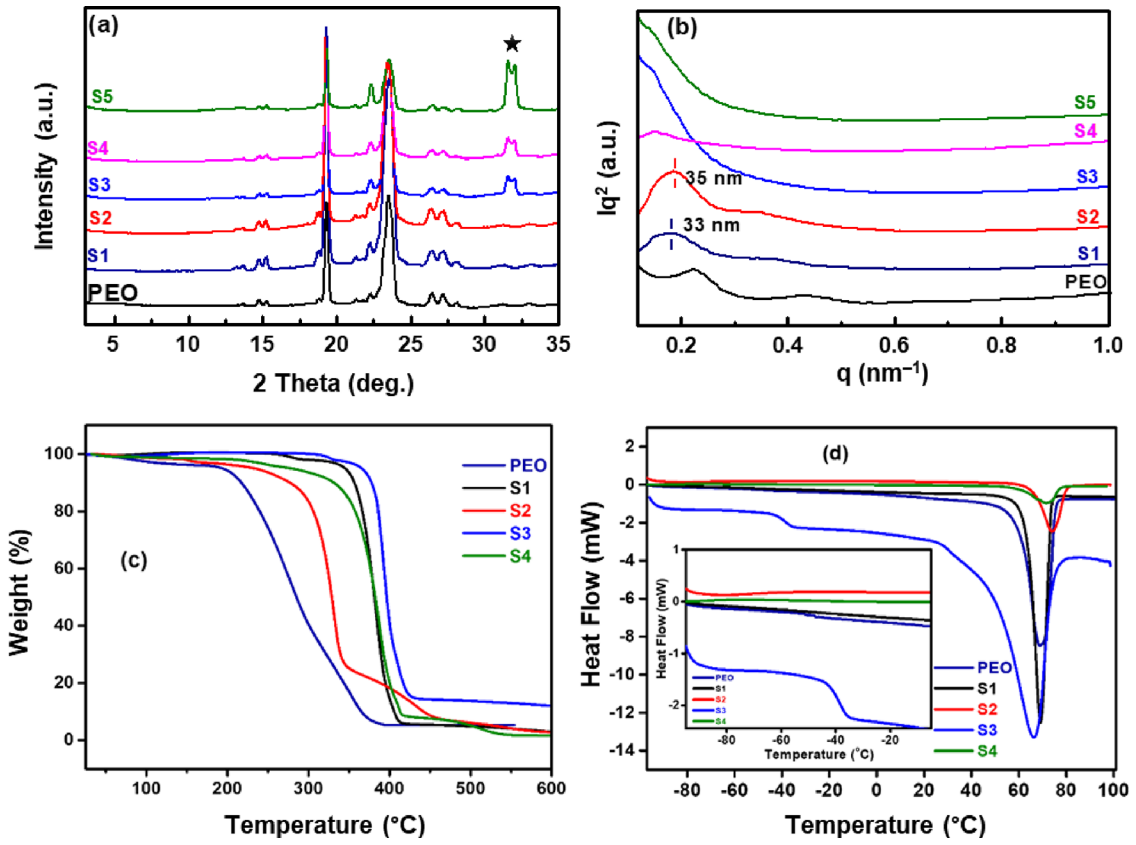

Figure 1. (a) WAXS and (b) SAXS patterns of the hybrid solid polymer electrolytes with different concentrations of $BaTiO_3$, viologen, and LiTFSI. (c) Thermogravimetric and (d) DSC traces of samples PEO, S1, S2, S3, and S4.

measurement. In this method, the deflection sensitivity of the probe was first calibrated on a clean, hard sample (Sapphire), and then a polystyrene with known modulus was used to calibrate the probe by adjusting the proper force set point of the tip and tip radius. After calibration, the tip was brought to measure the sample. Topography and QNM were measured at the same time in a way of 256 × 256 pixels/scan, i.e., 65,536 points of the sample were probed and their force curves were acquired. Young's modulus was derived from these force curves according the Derjaguin, Muller, Toropov (DMT) model.

The electrochemical characterization was performed in 2032-coin cells. To measure the ionic conductivity at different temperatures (0 to 70 °C), HSPE membranes were placed between two blocking electrodes and electrochemical impedance spectroscopy was performed by using a VMP3 (Biologic, France) in the 1 MHz to 100 mHz frequency range. To analyze the interfacial properties, nonblocking symmetric cells with Li/CPE/Li configuration were assembled, and the impedance vs time was measured after extended storage under open-circuit voltage at 60 °C.

To calculate the lithium transference number (t_{Li+}), a potentiostatic polarization method was employed as proposed by Bruce et al.[30]

$$t_{Li+} = \frac{I_{ss}(V - I_0R_0)}{I_0(V - I_{ss}R_{ss})} \quad (1)$$

where I_{ss} and I_0 represent the steady-state current and initial one, respectively. The R_0 and R_{ss} resistance values were obtained from EIS measurements before and after perturbation with a 10 mV DC voltage.

For the galvanostatic profiles, symmetric Li/sample S1 or sample S4/Li cells were assembled and were charged and discharged for 1 h in each cycle with a current density of 0.03 mA cm^{-2}. The area of the electrode was 1 cm^{-2}. The measurements could not be carried out for currents higher than 0.03 mA cm^{-2}.

The composite cathode was prepared by coating a slurry comprising 80 wt % lithium iron phosphate ($LiFePO_4$, 99,99%, Alfa Aesar), 10 wt % poly(vinylidene fluoride) (PVdF, Merck), and 10 wt % conducting carbon (Super P, Timcal) in *N*-methyl-2-pyrrolidone (NMP, Merck) on a cleaned aluminum foil by doctor blade method and then dried in an vacuum oven at 110 °C.[31] The active material loading was 3.0−3.5 mg cm^{-2}, and the density of the electrode is 1.53 g cm^{-3}. The HSPE membrane was placed between the composite cathode and lithium metal (Foote Minerals, USA) anode. A 2032-coin cell-type was assembled in an Ar gas-filled glove box (M Braun, Germany). Galvanostatic constant current charge−discharge curves were obtained between 2.5 and 4.2 V at 0.1 and 1-C rates using a battery tester (Arbin, USA).[27,32] Although the ionic conductivity studies were performed between 0 and 70 °C, the charge−discharge studies were performed at 60° C in order to avoid the melting of PEO. Sample S4 was subjected to a thorough electrochemical investigation as it was found to be the optimal candidate in terms of ionic conductivity.

For FESEM studies of the cathode materials, the 2032-type coin cells were carefully opened in an argon-filled glove box after cycling and the cathode materials were removed. Subsequently, the electrodes were washed with a combination of solvents EC: DMC, 1:1 (v/v), in order to remove possible traces of electrolyte salts.

3. RESULTS AND DISCUSSION

Understanding the effect of structure and morphology on the ionic transport properties is essential to optimize the design of solid polymer electrolytes. In these polymeric systems, the conductivity occurs in both the crystalline and amorphous states.[33] It was shown that the mobility of the amorphous chains creates a disordered state for better ion transport above the glass transition temperature (T_g) especially in semicrystalline SPEs and also that the crystalline phase can offer even

https://doi.org/10.1021/acsmaterialsau.3c00010
ACS Mater. Au XXXX, XXX, XXX−XXX

better ion transport and conductivity than the corresponding amorphous phase depending on the crystal structure, degree of crystallinity, and orientation.[34,35] The effects of lithium composition, BTO, and propionic acid viologen loading on the crystallinity of the HSPEs was assessed by combining XRD and DSC analyses. Figure 1a,b shows the wide- and small-angle X-ray scattering (WAXS/SAXS) patterns of PEO and its composites (as reported in Table 1).

PEO composites show X-ray reflections corresponding to the monoclinic crystal structure of PEO (Figure 1a).[36] The PEO matrix showed characteristic diffraction peaks at 19.3° and 23.4°/2θ, which were confirmed also in the HSPEs, thus revealing their partially crystalline structure. Very similar peak intensities are seen for the sample S2 when the viologen is added to the system PEO-salt, indicating that the degree of crystallinity did not change significantly with respect to S1. Instead, the intensity became weaker and broader with the addition of $BaTiO_3$ (sample S3), revealing a decrease in crystallinity of PEO. In composites containing $BaTiO_3$, additional X-ray reflections due to $BaTiO_3$ were observed (indicated by the asterisk in Figure 1a). The degree of crystallinity (DoC) of PEO was estimated by taking the ratio of crystalline peaks of PEO to the total area (area under the crystalline and amorphous peaks) in various samples,[37] and the values are summarized in Table 1.

The PEO-salt sample has a DoC of 73 ± 1% and, as the visual inspection of the pattern suggested, with the addition of viologen, the degree of crystallinity remains almost the same (71 ± 1%). The effect of the addition of BTO on the DoC was more relevant since a decrease of almost 10% was found in S3 compared to S1. Then, the DoC is very similar for S3 and S4 pointing out that the viologen has little or no effect on the crystallinity confirming the observation for S2 compared to S1. The sample S5 showed the lowest crystallinity as expected due to the high salt and filler content. The increase in the amorphous degree in hybrid polymer electrolytes originated by adding passive fillers is well known also because of its influence on the ionic conductivity, and it can be related to dipole−dipole or some acid−base Lewis-type interactions between PEO and $BaTiO_3$.[19]

The Lorentz-corrected SAXS patterns for the different samples are shown in Figure 1b. SAXS is a particularly useful technique to study the structure of nanocomposite polymers at the nanometer scale, which is of fundamental importance, since most of their properties greatly depend on the nanostructure.[38] In semicrystalline polymers like PEO the crystalline polymeric phase constituted by chain folded lamellar crystals coexists with a polymer-lithium phase (stoichiometric, crystalline) and an amorphous polymer-lithium phase. The crystalline lamellae are sort of building blocks similar to 2D sheets with nanometer thickness.[39,40] Pristine PEO shows SAXS peaks up to the third order indicating the ordered stacking of lamellar structure (alternate stacking of amorphous and crystalline regions) with the first-ordered peak at q = 0.22 nm^{-1}. The spacing estimated using Bragg's law ($L = 2\pi/q$) is 28 ± 1 nm, which is correspondent to the long period (L), the average sum of crystalline lamellae thickness, and amorphous layer thickness. The lamellar structure remained the same upon the addition of LiTFSI (sample S1) and LiTFSI/viologen (sample S2); however, the long period values increased slightly to 33 ± 1 and 35 ± 1 nm, respectively. SAXS analysis proved the similarity in terms of degree of crystallinity of PEO-LiTFSI (S1) and PEO-LiTFSI-viologen (S2) discussed above. The WAXS and SAXS data further confirmed that LiTFSI and viologen are dispersed in the amorphous phase of PEO at the molecular level without any aggregation (no X-ray peaks corresponding to the viologen are seen). On the other hand, for samples S3, S4, and S5 containing BTO, there is no evidence of the interference peak related to the crystalline nanodomains of PEO, although the corresponding WAXS patterns show the typical semicrystalline nature of the composites (Figure 1a). In general, the composites containing BTO showed strong scattering intensity at low q due to the scattering from the $BaTiO_3$ particles dispersed within the PEO matrix.[41] We could speculate that BTO particles agglomerated to some extent and segregated mainly in the amorphous region. Due to this, the amorphous regions might have an electron density similar to crystalline lamellae so that no SAXS peaks were visible. The presence of BTO could also have led to a new arrangement of the crystalline PEO phase likely inducing the formation of smaller PEO crystallites of different sizes, not spatially correlated, which could also cause the disappearance of the interference SAXS peak.

Figure 1 c shows the TGA profiles of the composite polymer electrolytes. For all the samples, the weight loss observed over a broad temperature range of 50−150 °C is attributed to moisture presence (or moisture thermal decomposition/degradation).[27] The irreversible decomposition starts at 205 °C for the PEO sample. Upon addition of LiTFSI (sample S1) and $BaTiO_3$ (sample S3) the thermal stability of the nanocomposites increased drastically. For instance, the decomposition starts at 350 and 370 °C for samples S1 and S3, respectively. This apparent increase in the thermal stability of S3 is attributed to the interaction of PEO with $BaTiO_3$.[41] It can therefore be speculated that the radicals generated during the degradation of the PEO matrix were effectively trapped by the well dispersed BTO nanofiller, showing the so called "shielding effect" that delayed the thermal degradation of the PEO matrix.[42] On the other hand, for samples S2 and S4 containing the viologen, the decomposition started at a lower temperature than for S1 and S3 though at a higher temperature than pure PEO.

DSC thermograms are presented in Figure 1d. Pristine PEO typically has a T_g well below 0 °C, in most cases between −80 and −40 °C, and melts at about 60 °C.[43] LiTFSI is considered among the best salts in terms of dissociation in PEO and additionally also acts as a plasticizer to reduce the amount of the crystalline phase of the polymeric host.[44] However, it is known that the ionic interactions between Li^+ and the oxygen are strong so that the PEO chains become less mobile inside the solid matrix and T_g increases with the salt content.[45] Sample S3 clearly shows a higher T_g with the onset at about −39.9 °C. Regarding the crystallization (endothermic melting peak), the presence of the viologen seemed to increase the melting temperature significantly while $BaTiO_3$ lowered the T_m. This trend in the T_m suggests that there is an influence of the additive type on thermal properties. The melting transition which is shifted to lower temperature can be explained by the Gibbs−Thomson equation,[46] which states that the melting point depression (in this case of bulk PEO) is inversely proportional to the crystal size. According to this, smaller crystals melt at lower T, which agrees well with the SAXS results for the S3 sample showing that BTO had an effect in limiting the PEO crystallite size. Despite this, the viologen eventually drove the T_m toward an overall increase also when the inorganic filler was added (sample S4).

https://doi.org/10.1021/acsmaterialsau.3c00010
ACS Mater. Au XXXX, XXX, XXX−XXX

3.1. Ionic Conductivity and Transference Number

Figure 2 presents the temperature dependence of the ionic conductivity for the samples containing different concentrations of lithium salt, BTO, and viologen.

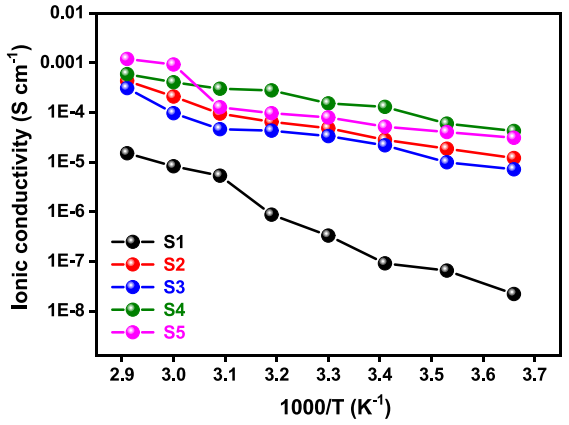

Figure 2. Arrhenius plot of ionic conductivity of HSPE samples (the solid line is shown as a guide to the eye).

The salt concentration was deliberately kept low (minimum EO:Li ratio of 30:1 in S5 corresponding to higher salt concentration) considering that high ionic conductivities were achieved previously for PEO SPE at low salt concentrations.[47,48] Furthermore, it is also of outmost importance to find a compromise between the ionic conductivity and the mechanical stability of the membrane, which usually is better for higher amount of the crystalline phase (lower salt concentration).

The ionic conductivity of the samples is of typical semicrystalline polymers where the low crystallinity and improved polymer chain mobility is reflected in a reduced influence of the chain mobility dependence to the ionic conductivity, thus leading to an Arrhenius-like behavior. In general, completely amorphous systems such as high molecular weight SPEs show Vogel–Tammann–Fulcher (VTF) behavior.[49] The semicrystalline state of our HSPEs can explain the change in slope that is clearly evident for samples S1 and S5 after 50 and 60 °C, respectively, in agreement with the DSC results. It is likely that extending the data collection well above the melting of the crystalline phase, the VTF behavior could be appreciated, as previously reported for other PEO based electrolytes.[49] It is obvious that the addition of each of the inert fillers had a significant impact on the ionic conductivity, which increased of almost two orders of magnitude in the investigated temperature range for both samples S2 and S3 having the same EO:Li ratio. As reported in Figure 2, the incorporation of both viologen and $BaTiO_3$ (sample S4 and S5) allowed further enhancement of ionic conductivity, and a value of 10^{-4} S cm^{-1} was achieved at room temperature for the sample S5. This behavior could be explained by a combination of positive effects such as the lower degree of crystallinity and smaller PEO crystal size because of BTO fillers, the variation of crystalline lamellae and amorphous layer thickness ratio by viologen addition, and the slightly lower EO:Li ratio. The inorganic particles, which have similar property of Lewis alkali, can weaken the polymer cation association and form an "ion-ceramic complex" system, thus facilitating dissociation of the lithium salt, increasing the number of free carriers and weakening the mutual relationship between O and Li^+.[50,51] The addition of viologen might have further increased the ionic conductivity synergistically due to the electrostatic interaction between its positive charge and TFSI anion (which is discussed in the later section). In general, our observations agree well with previously reported studies and match the interpretation that increasing the fraction of the amorphous phase in the hybrid polymer electrolyte improves the ionic conductivity thanks to a stronger participation of the polymer matrix to the transport process through segmental chain motions.

The ratio of migrating Li^+-ion to all migrating ionic species including the TFSI anion is termed as lithium transference number.[50] The lithium-ion transference number (t_{Li+}) is a critical parameter in evaluating the performance of the electrolyte in terms of energy density and rate capability, which are fundamental aspects for high power applications such as hybrid electric vehicles.[51] Figure 3 shows, as an

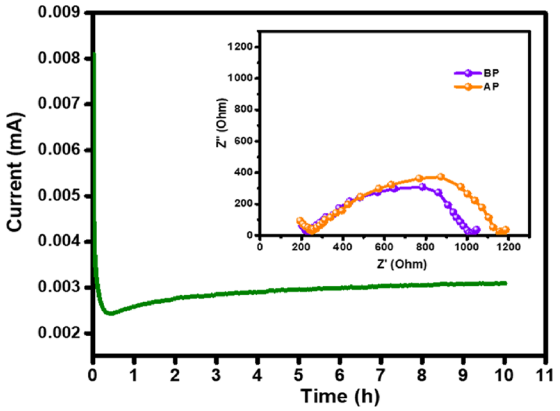

Figure 3. Chronoamperometric studies on the Li/HSPE/Li cell at 60 °C with sample S4 (BP, before perturbation; AP, after perturbation).

example, the chronoamperometric curves of sample S4 at 60 °C (see Figure SI 3a–c for S1, S2, and S3), and the inset presents the Nyquist plots before and after perturbation. Generally, the incorporation of metal oxides as inorganic filler not only improves the ionic conductivity but also has a positive effect on the lithium-ion transference number.[52] It is worth mentioning that the addition of ceramic fillers such as BTO can relax the polymer chains. Therefore, segmental motion is promoted under the interaction of inorganic fillers and polymer chains, accelerating dynamic processes between the segments.[52] The values of t_{Li+} are reported in Table 1. Typically, PEO-based SEs show a low Li^+ ion transference number (around 0.2) due to the strong coordination of the cations by the O atoms of the polyether chains (4 to 7 oxygen atoms coordinating lithium).[53] A lithium-ion transport number of 0.19 at 70 °C was previously reported for a $PEO_{20}LiPF_6$ electrolyte containing 5% of $BaTiO_3$ and of 0.14 at 80 °C for a PEO_{30}LiTFSI containing 10% of $BaTiO_3$.[54] The discharge rates of cells using lithium salts in polymer electrolytes are limited by depletion of the electrolyte in the porous electrode, resulting in a cell polarization problem, which in turn means a higher resistivity that might lead to a premature cell failure. In our work, a slightly greater value of t_{Li+} (0.23) has been measured for the $BaTiO_3$ and viologen added HSPE (S4 sample), which resulted higher if compared with filler-free (t_{Li+} = 0.16) and the single viologen or $BaTiO_3$-added membranes

https://doi.org/10.1021/acsmaterialsau.3c00010
ACS Mater. Au XXXX, XXX, XXX–XXX

(0.17 and 0.19, respectively) (Figure 3). Considering the viologen to PEO weight ratio, it has to be noticed that this ratio goes from 5.5% for S2 to 5.8% for S4 with an increasing trend, which is reflected in the t_{Li+} value. Ion diffusivity and ion concentration contribute to the transport of Li^+ ions in SEs. Examining the conductivity results, it can be noticed that in general, the effect due to the presence of the inorganic filler has relevant consequences on the ionic conductivity. In any case, the S3 sample, which does not contain viologen but BTO, has the lowest conductivity among the composites. In addition, viologen (see S2) also led to an enhancement of the ionic conductivity; however, looking at the results in Table 1, it did not help significantly in improving t_{Li+}. The combination of both BTO and viologen was more effective in enhancing the conductivity and the transport number at the same time. It was reported that clusters of LiTFSI can appear at high concentration of salt, resulting in a restricted cooperative motions of Li ions.[53] Ferroelectric ceramic powders possessing a permanent dipole are known to promote the dissociation of ion-ion pairs and ion-clusters in systems where there is a high tendency to association. However, the association tendency of LiTFSI is not very high, and the low salt concentration in our samples helped to prevent this issue, so that $BaTiO_3$ exerts a limited effect. The viologen is a dicationic salt, and molecular mobility of the 4,4′-bipyridinium cores was observed in some of them.[55]

Overall, the increased charges in the HSPEs promoting the dissociation of the lithium salt as well as hindering the formation of negatively charged complexes that might reduce the number of free Li^+ ions, together with the restricted motion of TFSI anion, led to an improvement of both ionic conductivity and t_{Li+} of the hybrid electrolytes. Additionally, the electrostatic repulsion between Li-ions and positive charges of viologen may further accelerate the lithium-ion movement in the HSPE. The electrostatic interaction between TFSI anions and positive charges of viologen is illustrated schematically in Figure 4. This further highlights the role of the viologen in the ionic transport in the HSPE. The sample S4 was found to be optimal in terms of ionic conductivity and t_{Li+} and therefore was selected for further galvanostatic current studies.

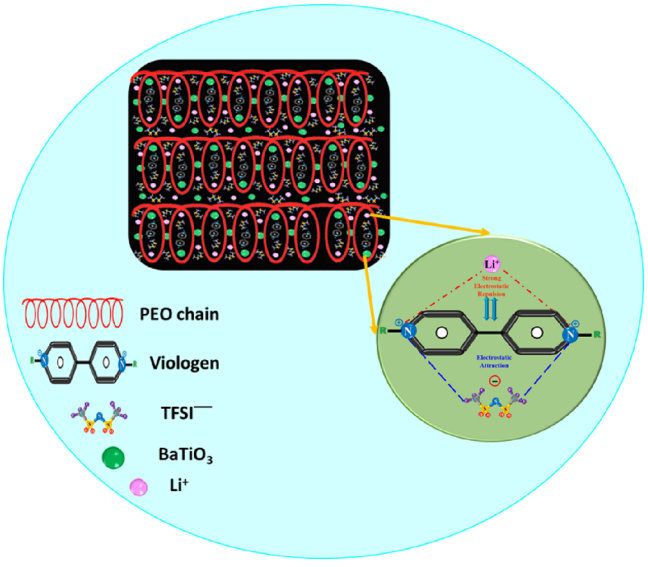

Figure 4. Schematic diagram of electrostatic attraction between viologen and TFSI anion.

3.2. Compatibility Studies of Li/HSPE/Li Symmetric Cell

The Li/electrolyte interfacial properties play a key role in determining the Coulombic efficiency and cyclability. Figure 5 shows the time dependence of the interfacial resistance "Ri" for the symmetric cell Li/HSPE/Li measured at 60 °C. All samples containing fillers (S2−S4) showed comparable interfacial resistance to the one of the PEO-salt system. However, despite the similar trend observed for all samples, the increase of "Ri" values as a function of storage time is more rapid/drastic for the sample S1 when compared to viologen and $BaTiO_3$-added samples. Apparently, the value of "Ri" is lower for the viologen-containing membrane (S2). The higher value for S3 than for S2 could be due to an increase in stiffness in the membrane due to the inorganic phase, which might likely compromise the interfacial contact. A similar resistance to S3 was observed for S4, for which the propionic acid viologen is added together with $BaTiO_3$.[59,60] Although more studies would be needed to clarify this behavior, this initial qualitative analysis seems to suggest that when $BaTiO_3$ is present, it has a prevalent effect over the organic filler, which seems not as effective as in S2 (for which is the only additive) to reduce the interfacial resistance of the hybrid electrolyte in contact with Li.

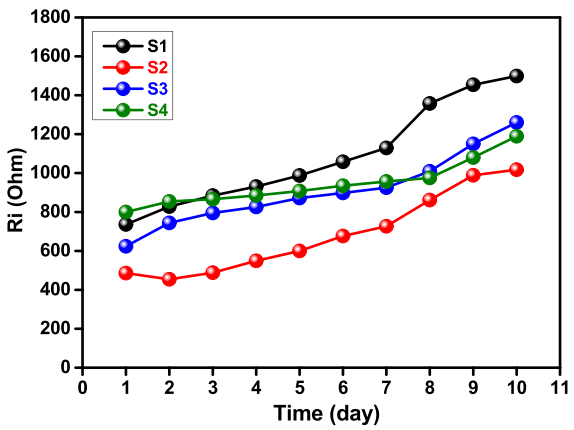

Figure 5. Variation of interfacial resistance "Ri" vs time for the symmetric cell comprising Li/HSPE/Li at 60 °C (the solid line is shown as a guide to the eye).

The voltage and current profiles of a galvanostatic experiment for the symmetric Li/sample S1 or sample S4/Li cells at 60 °C are shown in Figure SI 4. In both cases, no voltage fluctuations were observed while cycling, which normally occur due to the micro-short circuiting during the stripping and deposition of Li. However, a smooth voltage profile with less polarization up to 100 h is seen for the Li/Li symmetric cell containing the HSPE with viologen and $BaTiO_3$ (sample S4), indicating a steady and favorable environment for the ionic conduction inside the sample.

High-temperature and also low-temperature environments, where some kind of internal heating (for example upon Li plating at the anode) can raise the battery temperature, have much effect on the safety of LIBs. So far, the electrochemical stability of PEO has not yet been explored significantly in real battery systems.

https://doi.org/10.1021/acsmaterialsau.3c00010
ACS Mater. Au XXXX, XXX, XXX−XXX

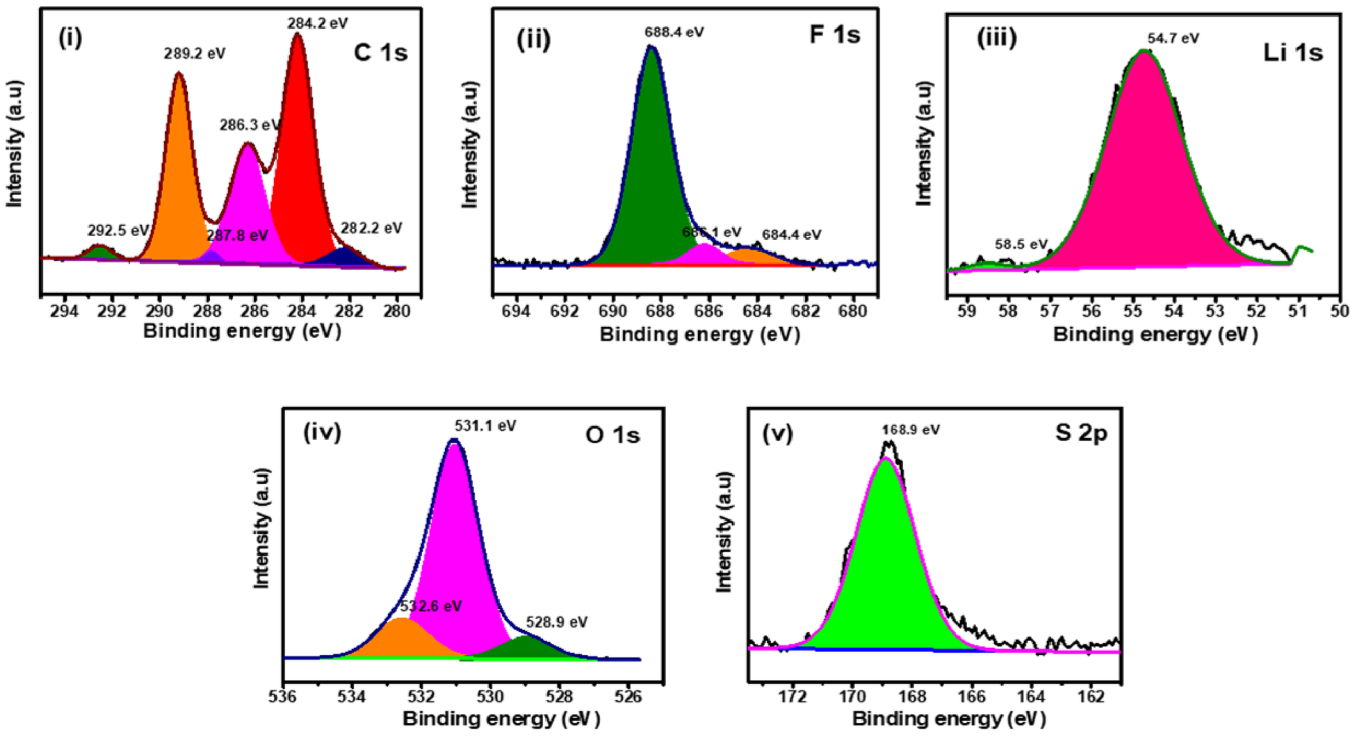

Figure 6. XPS spectra of the lithium surface upon contact with sample S4.

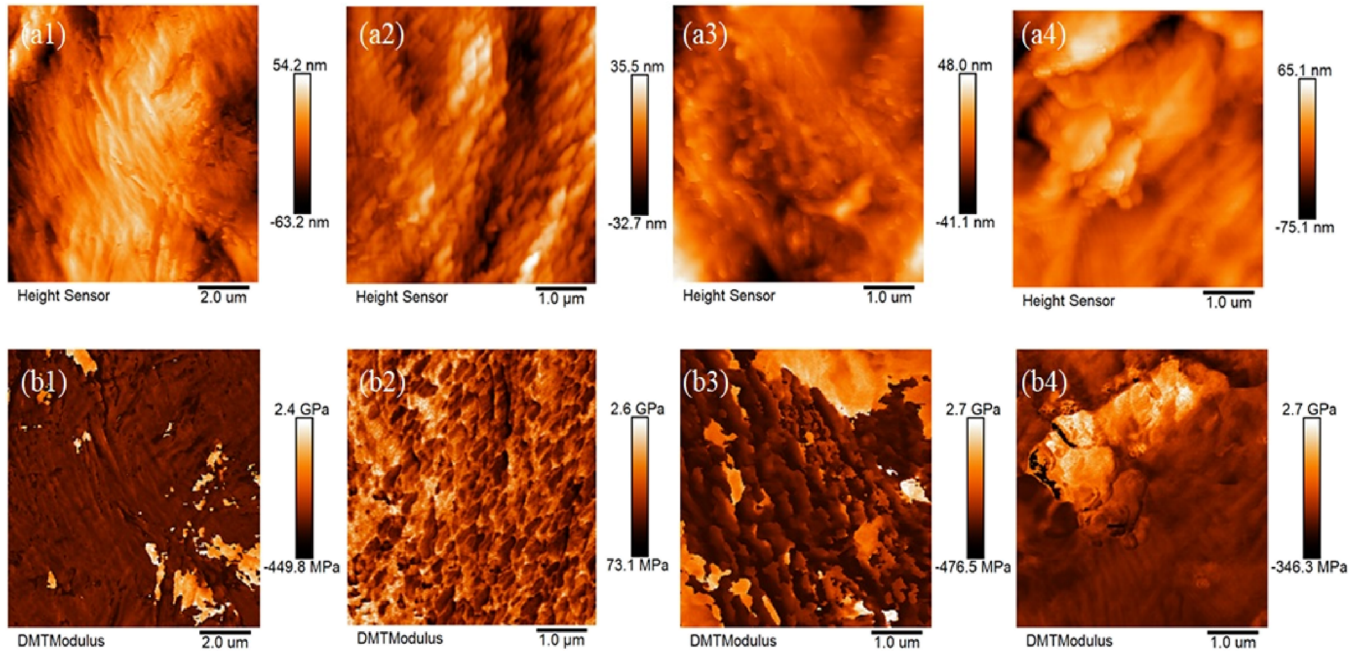

Figure 7. AFM measurement of the surface morphology and local Young's modulus of samples S2 (a1, b1), S3 (a2, b2), S4 (a3, b3), and S5 (a4, b4).

Although HSPE based on PEO might be promising for batteries working safely, some studies have shown that polyether might suffer extensive decomposition on the cathode.[56,57] For this, PEO is considered compatible mainly with $LiFePO_4$ and cannot work safely with 4 V class high energy density cathodes, such as $Li(Ni_xMn_yCo_{1-x-y})O_2$.[58] This kind of issue might be worsened at high operating temperatures. Specifically, the comprehensive effects of temperature on the cyclic aging rate are not completely understood. Many applications of industrial batteries face high temperatures such as in oil and gas exploration, industrial plants, etc., and LMBs that can work stably at high temperatures are highly desirable. In this regard, the composition of the lithium metal surface in contact with the HSPE in a cell stored at 60 °C, which might also be interesting to know in view of the development of LMBs, was investigated by XPS.

The symmetric cell Li/HSPE/Li containing the sample S4 was dismantled very carefully in an argon-filled glove box after

https://doi.org/10.1021/acsmaterialsau.3c00010
ACS Mater. Au XXXX, XXX, XXX−XXX

10 days of storage at 60 °C. During this storage time the interfacial resistance underwent only small variation after the assembly (see Figure 5). The polymeric film was peeled off from the metallic lithium and the side of lithium at the interface lithium/HSPE was analyzed. Figure 6i–v shows the high resolution XPS spectra of C 1s, F 1s, Li 1s, O 1s, and S 2p. Effects due to reactivity and sensitivity (to the environment conditions) make the effective implementation of surface technique analysis quite difficult and the obtained data have to be considered with caution. Usually the "as-received" lithium metal already comes with a native film on its surface, which is mainly composed of Li_2CO_3, LiOH, and Li_2O.[61] After contacting lithium with the polymer electrolyte, a passivation layer formed, and it was possible to identify differences in the composition of this thin film compared with the native film. The deconvoluted C 1s spectrum showed peaks at 292.5, 289.20, 286.3, 284.2, and 282.2 eV, which are assigned to C–F, C=O, C–O, C–C, and Li–C, respectively.[28,62] The F 1s spectrum showed that the peak at 688.4 eV represents C–F. In the Li 1s spectrum, the peak centered at 54.70 eV could be assigned to lithium hydroxide or alkoxide.[63,64] In the O 1s spectrum, the peaks observed at 528.9, 531.1, and 532.6 eV are assigned respectively to metal oxides, metal carbonates, and carbonyl or C=O bonds. An S 2p peak is also seen at 168.9 eV. The signals related to C 1s at 292.5 eV, F 1s at 688.4 eV, and S $2p_{3/2}$ at 168.9 eV indicate that TFSI is present on the surface.[65] The metal lithium/electrolyte interface resistance and stability are crucial for the successful development of LMBs. Longer storage time would be needed to ascertain the reactivity at the Li surface, in any case after a short storage at 60 °C unwanted reactions were likely limited, and the compounds already present as the passivation layer were still the main components on the metal surface.

3.3. Mechanical Properties

The evaluation of the mechanical properties of polymer electrolytes is often overlooked but quite important. In fact, the separators can undergo significant volume changes in contact with the electrodes during cell functioning. Also, they need to withstand a huge stress during cell manufacturing and there is a lot of interest in the development of stretchable batteries for wearables and for example for health monitoring systems. Very often, the mechanical stability is not sufficient at elevated temperatures where PEO conductivity improves, and large increases in the cell impedance are also found with cycling.

Figure 7 shows the AFM measurement of surface morphology and local Young's modulus of S2 to S5. The typical stripe structure of PEO can be found in S2 as shown in Figure 7a1,b1. The local Young's modulus of S2 shows a binary Young's modulus distribution, with a lower part of Young's modulus of ∼215 MPa and a higher part of Young's modulus of ∼1637 MPa. The lower one can be ascribed to PEO and the higher one can be ascribed to Viologen. Samples S4 and S5 show similar binary Young's modulus distribution due to the presence of Viologen. Meanwhile, sample S2 shows a relatively uniform structure with a mean Young's modulus of ∼1210 MPa, which might be due to the uniform coverage of PEO on $BaTiO_3$.

3.4. Charge–Discharge Cycling Studies

All-solid-state lithium cells were assembled with a Li-metal anode, $LiFePO_4$ cathode, and the HSPE S4 that was considered suitable for the cycling tests due to its good ionic conductivity. The typical galvanostatic charge–discharge cycling profiles of the $LiFePO_4$/HSPE/Li cell at 60 °C for S1 and S4 are compared in Figure 8a.

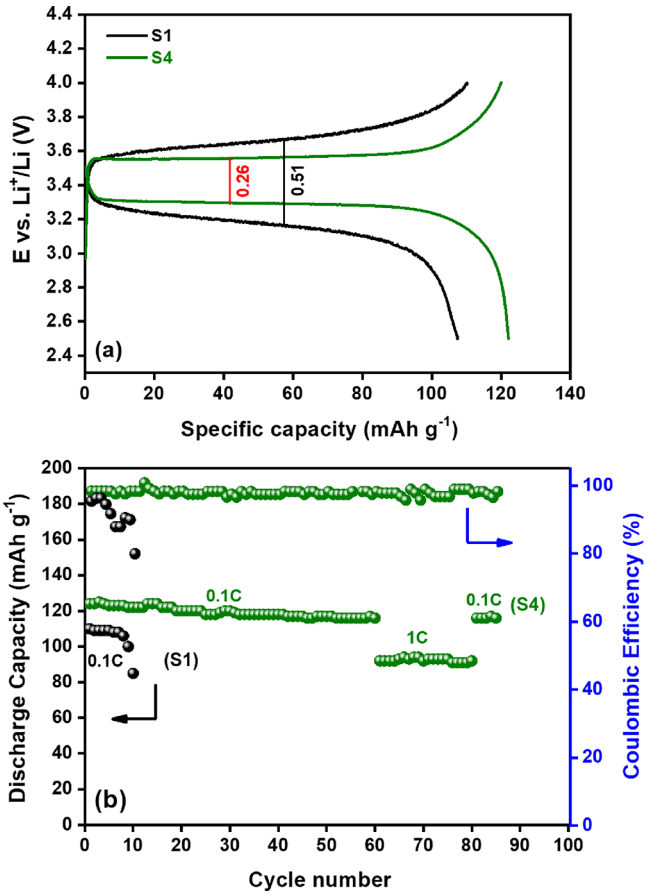

Figure 8. (a) Galvanostatic charge–discharge profiles of the Li/HSPE/$LiFePO_4$ cell with samples S1 and S4 at 60 °C; (b) discharge capacity as a function of cycle number at 0.1 and 1 C-rates at 60 °C.

For the cell containing S4, the charge–discharge profile between 2.5 and 4.0 V vs Li at 0.1 C-rate has a well-defined plateau at 3.55 V upon charging (de-lithiation) and about 3.3 V upon discharging (lithiation), which is a typical behavior of the $LiFePO_4$ electrode undergoing a reversible redox reaction with lithium.[52] The sample S1 shows a much higher overpotential along with a slope change not well defined at the end of the redox process. Specifically, sample S1 shows an overpotential of 0.51 V when the capacity reached 60 mAh/g, which is almost twice the one of sample S4, constantly at 0.26 V. As seen in the previous sections, S1 had a much higher interfacial resistance with lithium that probably originated this difference with S4, in agreement with other published results.[66] Figure 8b shows the plot of specific capacity as a function of cycle number at 0.1 and 1 C-rate. The cell with S1 had a very rapid capacity decay during the first 10 cycles at 0.1 C-rate, while the other one with S4 delivered an initial discharge capacity of 123 mAh g^{-1} and similar for the first 60 cycles with 94% Coulombic efficiency. The capacity of this cell was stable even at cycling at higher C-rate (1 C), which evidences the good mechanical stability of the electrode during the Li^+-ion intercalation/de-intercalation process, stable interfacial contact, efficient charge transport between the electrode and the polymer electrolyte, and excellent reversibility after the initial surface reactions.[67] At 1 C-rate, the discharge capacity is

https://doi.org/10.1021/acsmaterialsau.3c00010
ACS Mater. Au XXXX, XXX, XXX–XXX

reduced to 90 mAh g^{-1}. The reduced discharge capacity at higher current is ascribed to the low electronic conductivity of electrode active material and limited diffusion of Li^+-ions into its structure, due to the not engineered interface between the binder and the active material, which was apart the scope of the work. The cell restored initial capacity again at the 0.1 C-rate from the 81st cycle demonstrating the retaining of structural stability of the cathode and the good performance of the electrolyte. After 80 cycles, the cell delivered a discharge capacity of 119 mAh g^{-1} with a capacity retention of 96% (i.e., from 123 to 119 mAh g^{-1}).[68] On the other hand, the Li/$LiFePO_4$ cells with samples S2 and S3 offered inferior discharge capacity (Figure SI 5) and was attributed to the lower ionic conductivity of the solid polymeric membranes.[69,70] The cycled cells were dismantled and were subjected to FE-SEM analysis. Figure SI 6a–c shows the FE-SEM images of the cathode materials as prepared, after 20 and 100 cycles at 1 C-rate. Apparently, upon cycling the cathode materials became loosely packed and developed to form some sort of isles. However, no cracks are seen on the surface of the cathode materials, which accounts for the stable behavior upon cycling.

4. CONCLUSIONS

Organic materials such as viologens can offer promising solutions to enhance performance and sustainability of current technologies. In this work, we have successfully synthesized the 1,1′-bis(2 carboxyethyl)-4,4′-bipyridine-1,1′ dibromide viologen as confirmed by NMR. Crystallinity remarkably affects the properties of polymer electrolytes and hinders ionic conductivity. In an effort to overcome the major limitations in the ion transport of PEO-based SEs, thin and flexible HSPEs incorporating LiTFSI, viologen and $BaTiO_3$ were prepared by simple hot-press. The chosen low salt concentration allowed us to control the crystalline/amorphous fraction of PEO, which is essential for achieving good mechanical properties, without compromising the ionic conductivity, that was also boosted by the inorganic filler, $BaTiO_3$. For the compositions assessed, a 5% content of both viologen and BTO were sufficient to obtain very good ionic conductivity of 1.5×10^{-4} S cm^{-1} at 25 °C and this HSPE was used in the all-solid metal battery. In the voltage range of 2.5–4.0 V at 60 °C, the Li/HSPE/$LiFePO_4$ cell retained an initial discharge capacity of 123 mAh g^{-1} at 0.1 C for 60 cycles with a Coulombic efficiency of 94–98%. Even after excursions at 1 C-rate, the cell operated with good Coulombic efficiency and no visible loss of capacity. This excellent performance can be related to the small cell polarization likely due to a good contact between the polymer and the electrode and the sufficient transference number. The viologen helped in inhibiting the reactivity at the interfaces and was beneficial for the ion transport. The work presented herein introduces a way of combining viologen and inert fillers for modifying the properties of solid polymer electrolytes, and the results prove the potential of HSPEs for future all solid-state lithium metal batteries.

■ ASSOCIATED CONTENT

Supporting Information

The Supporting Information is available free of charge at https://pubs.acs.org/doi/10.1021/acsmaterialsau.3c00010.

Preparation of viologen; (Figure SI 1) spectra of propionic viologen (a) ^{1}H NMR (b)^{13}C NMR, and (c) DEPT spectrum of propionic acid viologen; (Figure SI 2) EDX of hybrid solid polymer electrolyte (sample S4); (Figure SI 3) chronoamperometric studies on Li/HSPE/Li cell at 60 °C for samples (a) S1, (b) S2, and (c) S3 (BP-Before perturbation, AP-After perturbation); (Figure SI 4) galvanostatic profiles of the symmetric Li/Li cells at 60 °C: (a) with sample S4 and (b) with sample S1, current density = 0.03 mA cm^{-2}; (Figure SI 5) discharge capacity as a function of cycle number of $LiFePO_4$/HSPE/Li cell at 0.1 C-rate at 60 °C cycled with samples S2 and S3; (Figure SI 6) FESEM images of $LiFePO_4$ cathode (a) as prepared, (b) after 20 cycles, and (c) after 100 cycles at 1 C-rate (PDF)

■ AUTHOR INFORMATION

Corresponding Authors

Claudio Gerbaldi − *GAME Laboratory, Department of Applied Science and Technology (DISAT), Politecnico di Torino, Torino 10129, Italy; National Reference Center for Electrochemical Energy Storage (GISEL)—INSTM, Firenze 50121, Italy;* orcid.org/0000-0002-8084-0143; Email: claudio.gerbaldi@polito.it

Arul Manuel Stephan − *CSIR- Central Electrochemical Research Institute, Karaikudi 630 003, India;* Email: amstephan@cecri.res.in

Authors

Natarajan Angulakhsmi − *Ningbo Institute of Materials Technology & Engineering, Chinese Academy of Sciences, Zhejiang 315201, China;* orcid.org/0000-0002-6289-7963

Bebin Ambrose − *CSIR- Central Electrochemical Research Institute, Karaikudi 630 003, India;* Present Address: Academy of Scientific and Innovative Research (AcSIR), Ghaziabad 201,002, India (S.S.)

Swamickan Sathya − *CSIR- Central Electrochemical Research Institute, Karaikudi 630 003, India;* Present Address: Academy of Scientific and Innovative Research (AcSIR), Ghaziabad 201,002, India (S.S.)

Murugavel Kathiresan − *CSIR- Central Electrochemical Research Institute, Karaikudi 630 003, India;* orcid.org/0000-0002-1208-5879

Gabriele Lingua − *GAME Laboratory, Department of Applied Science and Technology (DISAT), Politecnico di Torino, Torino 10129, Italy; National Reference Center for Electrochemical Energy Storage (GISEL)—INSTM, Firenze 50121, Italy*

Stefania Ferrari − *Department of Pharmacy, Università di Chieti-Pescara "G. d'Annunzio", Chieti 66100, Italy; National Reference Center for Electrochemical Energy Storage (GISEL)—INSTM, Firenze 50121, Italy*

Erathimmanna Bhoje Gowd − *Materials Science and Technology Division, CSIR-National Institute for Interdisciplinary Science and Technology, Trivandrum, Kerala 695 019, India*

Wenyang Wang − *Ningbo Institute of Materials Technology & Engineering, Chinese Academy of Sciences, Zhejiang 315201, China*

Cai Shen − *Ningbo Institute of Materials Technology & Engineering, Chinese Academy of Sciences, Zhejiang 315201, China;* orcid.org/0000-0001-5825-4028

https://doi.org/10.1021/acsmaterialsau.3c00010
ACS Mater. Au XXXX, XXX, XXX−XXX

Giuseppe Antonio Elia − *GAME Laboratory, Department of Applied Science and Technology (DISAT), Politecnico di Torino, Torino 10129, Italy; National Reference Center for Electrochemical Energy Storage (GISEL)—INSTM, Firenze 50121, Italy;* orcid.org/0000-0001-6790-1143

Complete contact information is available at: https://pubs.acs.org/10.1021/acsmaterialsau.3c00010

Author Contributions

CRediT: **Natarajan Angulakshmi** data curation (equal), formal analysis (equal), investigation (equal), methodology (equal), writing-original draft (equal); **Bebin Ambrose** data curation (equal), formal analysis (equal), investigation (equal); **Swamickan Sathya** data curation (equal), formal analysis (equal), methodology (equal); **Murugavel Kathiresan** data curation (equal), methodology (equal), writing-original draft (equal); **Gabriele Lingua** formal analysis (equal), investigation (equal), writing-review & editing (equal); **Stefania Ferrari** data curation (equal), validation (equal), writing-original draft (equal), writing-review & editing (equal); **Erathimmanna Bhoje Gowd** investigation (equal), methodology (equal), writing-review & editing (equal); **Wenyang Wang** data curation (equal), investigation (equal), writing-review & editing (equal); **Cai Shen** data curation (equal), investigation (equal), writing-review & editing (equal); **Giuseppe Antonio Elia** data curation (equal), methodology (equal), writing-review & editing (equal); **Claudio Gerbaldi** conceptualization (equal), supervision (equal), validation (equal), writing-original draft (equal), writing-review & editing (equal); **Arul Manuel Stephan** conceptualization (equal), data curation (equal), formal analysis (equal), resources (equal), supervision (equal), writing-original draft (equal), writing-review & editing (equal).

Notes

The authors declare no competing financial interest.

■ ACKNOWLEDGMENTS

The authors S.S. and A.B. gratefully acknowledge CSIR and UGC for the financial assistance. This study was carried out within the MOST e Sustainable Mobility Center and received funding from the European Union Next-GenerationEU (PIANO NAZIONALE DI RIPRESA E RESILIENZA (PNRR) e MISSIONE 4 COMPONENTE 2, INVESTIMENTO 1.4 e D.D. 1033 17/06/2022, CN00000023). This manuscript reflects only the authors' views and opinions; neither the European Union nor the European Commission can be considered responsible for them. Part of this work was carried out within the activities "Ricerca Sistema Elettrico" funded through contributions to research and development by the Italian Ministry of Economic Development. G.A.E. and C.G. acknowledge financial support by the Si-DRIVE Project (http://sidrive2020.eu/), which received funding from the European Union's Horizon 2020 research and innovation program under Grant Agreement no. 814464.

■ REFERENCES

(1) Dunn, B.; Kamath, H.; Tarascon, J. M. Electrical Energy Storage for the Grid: A Battery of Choices. *Science* **2011**, *334*, 928−935.
(2) Goodenough, J. B. How We Made the Li-ion Rechargeable Battery. *Nat. Electron.* **2018**, *1*, 204−204.
(3) Goodenough, J. B. Evolution of Strategies for Modern Rechargeable Batteries. *Acc. Chem. Res.* **2013**, *46*, 1053−1061.
(4) Goodenough, J. B.; Park, K. S. The Li-Ion Rechargeable Battery: A Perspective. *J. Am. Chem. Soc.* **2013**, *135*, 1167−1176.
(5) Liu, K.; Liu, Y.; Lin, D.; Pei, A.; Cui, Y. Materials for Lithium-ion Battery Safety. *Sci. Adv.* **2018**, *4*, No. eaas9820.
(6) Cheng, X.-B.; Zhang, R.; Zhao, C.-Z.; Zhang, Q. Toward Safe Lithium Metal Anode in Rechargeable Batteries: A Review. *Chem. Rev.* **2017**, *117*, 10403−10473.
(7) Liu, W.; Song, M. S.; Kong, B.; Cui, Y. Flexible and stretchable energy storage: Recent Advances and Future Perspectives. *Adv. Mater.* **2017**, *29*, No. 1603436.
(8) Sun, C.; Liu, J.; Gong, Y.; Wilkinson, D. P.; Zhang, J. Recent Advances in All-solid-state Rechargeable Lithium Batteries. *Nano Energy* **2017**, *33*, 363−386.
(9) Falco, M.; Ferrari, S.; Appetecchi, G. B.; Gerbaldi, C. Managing transport properties in composite electrodes/electrolytes for all-solid-state lithium-based batteries. *Mol. Syst. Des. Eng.* **2019**, *4*, 850−871.
(10) Manuel Stephan, A.; Nahm, K. S. Review on composite polymer electrolytes for lithium batteries. *Polymer* **2006**, *47*, 5952−5964.
(11) Fenton, D. E.; Parker, J. M.; Wright, P. V. Complexes of alkali metal ions with poly(ethylene oxide). *Polymer* **1973**, *14*, 589−589.
(12) Fan, L.; Nan, C.-W.; Zhao, S. Effect of modified SiO_2 on the properties of PEO-based polymer electrolytes. *Solid State Ionics* **2003**, *164*, 81−86.
(13) Yang, Z.; Fan, J.; Xu, W.; Yang, Z.; Zeng, J.; Cao, X. Solvation-Free Fabrication of PEO/LiTFSI/SiO_2 Composite Electrolyte Membranes with High Ionic Conductivity Based on a Novel Elongational Flow Field. *Ind. Eng. Chem. Res.* **2022**, *61*, 4850−4859.
(14) D'Epifanio, A.; Serraino Fiory, F.; Licoccia, S.; Traversa, E.; Scrosati, B.; Croce, F. Metallic-lithium, $LiFePO_4$-based polymer battery using PEO—ZrO_2 nanocomposite polymer electrolyte. *J. Appl. Electrochem.* **2004**, *34*, 403−408.
(15) Jayathilaka, P. A. R. D.; Dissanayake, M. A. K. L.; Albinsson, I.; Mellander, B.-E. Effect of nano-porous Al_2O_3 on thermal, dielectric and transport properties of the $(PEO)_9$ LiTFSI polymer electrolyte system. *Electrochim. Acta* **2002**, *47*, 3257−3268.
(16) Zewde, B. W.; Admassie, S.; Zimmermann, J.; Isfort, C. S.; Scrosati, B.; Hassoun, J. Enhanced Lithium Battery with Polyethylene Oxide-Based Electrolyte Containing Silane−Al_2O_3 Ceramic Filler. *ChemSusChem* **2013**, *6*, 1400−1405.
(17) Lin, C. W.; Hung, C. L.; Venkateswarlu, M.; Hwang, B. J. Influence of TiO_2 nano-particles on the transport properties of composite polymer electrolyte for lithium-ion batteries. *J. Power Sources* **2005**, *146*, 397−401.
(18) Sun, H.-Y.; Sohn, H.-J.; Yamamoto, O.; Takeda, Y.; Imanishi, N. Enhanced Lithium-Ion Transport in PEO-Based Composite Polymer Electrolytes with Ferroelectric $BaTiO_3$. *J. Electrochem. Soc.* **1999**, *146*, 1672.
(19) Capiglia, C.; Yang, J.; Imanishi, N.; Hirano, A.; Takeda, Y.; Yamamoto, O. Composite polymer electrolyte: the role of filler grain size. *Solid State Ionics* **2002**, *154-155*, 7−14.
(20) Dong, P.; Zhang, X.; Han, K. S.; Cha, Y.; Song, M.-K. Deep eutectic solvent-based polymer electrolyte for solid-state lithium metal batteries. *J. Energy Chem.* **2022**, *70*, 363−372.
(21) Keller, M.; Varzi, A.; Passerini, S. Hybrid electrolytes for lithium metal batteries. *J. Power Sources* **2018**, *392*, 206−225.
(22) Striepe, L.; Baumgartner, T. Viologens and Their Application as Functional Materials. *Chem. − Eur. J.* **2017**, *23*, 16924−16940.
(23) Madasamy, K.; Velayutham, D.; Suryanarayanan, V.; Kathiresan, M.; Ho, K.-C. Viologen-based electrochromic materials and devices. *J. Mater. Chem. C* **2019**, *7*, 4622−4637.
(24) Ding, J.; Zheng, C.; Wang, L.; Lu, C.; Zhang, B.; Chen, Y.; Li, M.; Zhai, G.; Zhuang, X. Viologen-inspired functional materials: synthetic strategies and applications. *J. Mater. Chem. A* **2019**, *7*, 23337−23360.
(25) Kathiresan, M.; Ambrose, B.; Angulakshmi, N.; Mathew, D. E.; Sujatha, D.; Stephan, A. M. Viologens: A versatile organic molecule for energy storage applications. *J. Mater. Chem. A* **2021**, *9*, 27215−27233.

(26) Han, H.-B.; Zhou, S.-S.; Zhang, D.-J.; Feng, S.-W.; Li, L.-F.; Liu, K.; Feng, W.-F.; Nie, J.; Li, H.; Huang, X.-J.; Armand, M.; Zhou, Z.-B. Lithium bis(fluorosulfonyl)imide (LiFSI) as conducting salt for nonaqueous liquid electrolytes for lithium-ion batteries: Physicochemical and electrochemical properties. *J. Power Sources* **2011**, *196*, 3623−3632.
(27) Angulakshmi, N.; Thomas, S.; Nair, J. R.; Bongiovanni, R.; Gerbaldi, C.; Stephan, A. M. A Cycling Profile of Innovative Nanochitin-Incorporated Poly(ethylene oxide) Based Electrolytes for Lithium Batteries. *J. Power Sources* **2013**, *228*, 294.
(28) Sathya, S.; Angulakshmi, N.; Ahn, J.-H.; Kathiresan, M.; Stephan, A. M. Influence of additives on the electrochemical and interfacial properties of SiO_x-based anode materials for lithium−sulfur batteries. *Langmuir* **2022**, *38*, 2423−2434.
(29) Baer, D. R.; Artyushkova, K.; Cohen, H.; Easton, C. D.; Engelhard, M.; Gengenbach, T. R.; Greczynski, G.; Mack, P.; Morgan, D. J.; Roberts, A. XPS guide: Charge neutralization and binding energy referencing for insulating samples. *J. Vac. Sci. Technol., A* **2020**, *38*, 031204−031219.
(30) Evans, J.; Vincent, C. A.; Bruce, P. G. Electrochemical Measurement of Transference Numbers in Polymer Electrolytes. *Polymer* **1987**, *28*, 2324−2328.
(31) Meligrana, G.; Gerbaldi, C.; Tuel, A.; Bodoardo, S.; Penazzi, N. Hydrothermal synthesis of high surface $LiFePO_4$ powders as cathode for Li-ion cells. *J. Power Sources* **2006**, *160*, 516−522.
(32) Gerbaldi, C.; Nair, J. R.; Kulandainathan, M. A.; Kumar, R. S.; Ferrara, C.; Mustarelli, P.; Stephan, A. M. Innovative high performing metal organic framework (MOF)-laden nanocomposite polymer electrolytes for all-solid-state lithium batteries. *J. Mater. Chem. A* **2014**, *2*, 9948−9954.
(33) Gadjourova, Z.; Andreev, Y. G.; Tunstall, D. P.; Bruce, P. G. Ionic conductivity in crystalline polymer electrolytes. *Nature* **2001**, *412*, 520−523.
(34) Lin, D.; Liu, W.; Liu, Y.; Lee, H. R.; Hsu, P.-C.; Liu, K.; Cui, Y. High Ionic Conductivity of Composite Solid Polymer Electrolyte via In Situ Synthesis of Monodispersed SiO_2 Nanospheres in Poly(ethylene Oxide). *Nano Lett.* **2016**, *16*, 459−465.
(35) Capiglia, C.; Saito, Y.; Yamamoto, H.; Kageyama, H.; Mustarelli, P. Transport Properties and Microstructure of Gel Polymer Electrolytes. *Electrochim. Acta* **2000**, *45*, 1341−1345.
(36) Cheng, S.; Smith, D. M.; Li, C. Y. How does nanoscale crystalline structure affect ion transport in solid polymer electrolytes? *Macromolecules* **2014**, *47*, 3978−3986.
(37) Rosely, C. V. S.; Joseph, A. M.; Leuteritz, A.; Gowd, E. B. Phytic Acid Modified Boron Nitride Nanosheets as Sustainable Multifunction Nanofillers for Enhanced Properties of Poly(L-lactide). *ACS Sustainable Chem. Eng.* **2020**, *8*, 1868−1878.
(38) Turković, A.; Dubček, P.; Juraić, K.; Drašner, A.; Bernstorff, S. SAXS Studies of TiO_2 Nanoparticles in Polymer Electrolytes and in Nanostructured Films. *Materials* **2010**, *3*, 4979−4993.
(39) Ribeiro, R.; Silva, G. G.; Mohallem, N. D. S. A comparison of ionic conductivity, thermal behaviour and morphology in two polyether−LiI−$LiAl_5O_8$ composite polymer electrolytes. *Electrochim. Acta* **2001**, *46*, 1679−1686.
(40) He, Z.; Chen, L.; Zhang, B.; Liu, Y.; Fan, L. Z. Flexible poly (ethylene carbonate)/garnet composite solid electrolyte reinforced by poly (vinylidene fluoride-hexafluoropropylene) for lithium metal batteries. *J. Power Sources* **2018**, *392*, 232−238.
(41) Angulakshmi, N.; Kar, G. P.; Bose, S.; Gowd, E. B.; Thomas, S.; Stephan, A. M. A high performance BaTiO3-grafted-GO-laden poly(ethylene oxide)-based membrane as an electrolyte for all-solid lithium batteries. *Mater. Chem. Front.* **2017**, *1*, 269−277.
(42) Thomas, S. P.; Thomas, S.; Bandyopadhyay, S. Polystyrene−Calcium Phosphate Nanocomposites: Preparation, Morphology, and Mechanical Behavior. *J. Phys. Chem. C* **2009**, *113*, 97−104.
(43) Stolwijk, N. A.; Heddier, C.; Reschke, M.; Wiencierz, M.; Bokeloh, J.; Wilde, G. Salt concentration dependence of the glass transition temperature in PEO−NAI and PEO−LITFSI polymer electrolytes. *Macromolecules* **2013**, *46*, 8580−8588.
(44) Gorecki, W.; Roux, C.; Clémancey, M.; Armand, M.; Belorizky, E. NMR and Conductivity Study of Polymer Electrolytes in the Imide Family: P(EO)/Li[$N(SO_2C_nF_{2n+1})(SO_2C_mF_{2m+1})$]. *ChemPhysChem* **2002**, *3*, 620−625.
(45) Angulakhsmi, N.; Thomas, S.; Nair, J. R.; Bongiovanni, R.; Gerbaldi, C.; Stephan, A. M. Cycling profile of innovative nanochitin-incorporated poly (ethylene oxide) based electrolytes for lithium batteries. *J. Power Sources* **2013**, *228*, 294−299.
(46) Jackson, C. L.; McKenna, G. B. The melting behavior of organic materials confined in porous solids. *J. Chem. Phys.* **1990**, *93*, 9002−9011.
(47) Daigle, J.-C.; Vijh, A.; Hovington, P.; Gagnon, C.; Hamel-Pâquet, J.; Verreault, S.; Turcotte, N.; Clément, D.; Guerfi, A.; Zaghib, K. Lithium battery with solid polymer electrolyte based on comb-like copolymers. *J. Power Sources* **2015**, *279*, 372−383.
(48) Stolwijk, N. A.; Wiencierz, M.; Heddier, C.; Kösters, J. What Can We Learn from Ionic Conductivity Measurements in Polymer Electrolytes? A Case Study on Poly(ethylene oxide) (PEO)−NaI and PEO−LiTFSI. *J. Phys. Chem. B* **2012**, *116*, 3065−3074.
(49) Mindemark, J.; Lacey, M. J.; Bowden, T.; Brandell, D. Beyond PEO-Alternative host materials for Li^+-conducting solid polymer electrolytes. *Prog. Polym. Sci.* **2018**, *81*, 114−143.
(50) Chen, F.; Yang, D.; Zha, W.; Zhu, B.; Zhang, Y.; Li, J.; Gu, Y.; Shen, Q.; Zhang, L.; Sadoway, D. R. Solid polymer electrolytes incorporating cubic $Li_7La_3Zr_2O_{12}$ for all-solid-state lithium rechargeable batteries. *Electrochim. Acta* **2017**, *258*, 1106−1114.
(51) Liang, Y. F.; Deng, S. J.; Xia, Y.; Wang, X. L.; Xia, X. H.; Wu, J. B.; Gu, C. D.; Tu, J. P. A superior composite gel polymer electrolyte of $Li_7La_3Zr_2O_{12}$-poly (vinylidene fluoride-hexafluoropropylene)-(PVDF-HFP) for rechargeable solid-state lithium ion batteries. *Mater. Res. Bull.* **2018**, *102*, 412−417.
(52) Piana, G.; Bella, F.; Geobaldo, F.; Meligrana, G.; Gerbaldi, C. PEO/LAGP hybrid solid polymer electrolytes for ambient temperature lithium batteries by solvent-free, "one pot" preparation. *J. Energy Storage* **2019**, *26*, No. 100947.
(53) Molinari, N.; Mailoa, J. P.; Kozinsky, B. Effect of salt concentration on ion clustering and transport in polymer solid electrolytes: a molecular dynamics study of PEO−LiTFSI. *Chem. Mater.* **2018**, *30*, 6298−6306.
(54) Takeda, Y.; Imanishi, N.; Yamamoto, O. Developments of the advanced all-solid-state polymer electrolyte lithium secondary battery. *Electrochemistry* **2009**, *77*, 784−797.
(55) Bhowmik, P. K.; Noori, O.; Chen, S. L.; Han, H.; Fisch, M. R.; Robb, C. M.; Variyam, A.; Martinez-Felipe, A. Ionic liquid crystals: Synthesis and characterization via NMR, DSC, POM, X-ray diffraction and ionic conductivity of asymmetric viologen bistriflimide salts. *J. Mol. Liq.* **2021**, *328*, No. 115370.
(56) Lingua, G.; Grysan, P.; Vlasov, P. S.; Verge, P.; Shaplov, A. S.; Gerbaldi, C. Unique Carbonate-Based Single Ion Conducting Block Copolymers Enabling High-Voltage, All-Solid-State Lithium Metal Batteries. *Macromolecules* **2021**, *54*, 6911−6924.
(57) Zhai, H.; Gong, T.; Xu, B.; Cheng, Q.; Paley, D.; Qie, B.; Jin, T.; Fu, Z.; Tan, L.; Lin, Y.-H.; Nan, C.-W.; Yang, Y. Stabilizing Polyether Electrolyte with a 4 V Metal Oxide Cathode by Nanoscale Interfacial Coating. *ACS Appl. Mater. Interfaces* **2019**, *11*, 28774−28780.
(58) Kobayashi, T.; Kobayashi, Y.; Tabuchi, M.; Shono, K.; Ohno, Y.; Mita, Y.; Miyashiro, H. Oxidation reaction of polyether-based material and its suppression in lithium rechargeable battery using 4 V class cathode, LiNi1/3Mn1/3Co1/3O2. *ACS Appl. Mater. Interfaces* **2013**, *5*, 12387−12393.
(59) Tatara, R.; Karayaylali, P.; Yu, Y.; Zhang, Y.; Giordano, L.; Maglia, F.; Jung, R.; Schmidt, J. P.; Lund, I.; Shao-Horn, Y. The Effect of Electrode-Electrolyte Interface on the Electrochemical Impedance Spectra for Positive Electrode in Li-Ion Battery. *J. Electrochem. Soc.* **2019**, *166*, A5090−A5098.
(60) Sharova, V.; Moretti, A.; Diemant, T.; Varzi, A.; Behm, R. J.; Passerini, S. Comparative study of imide-based Li salts as electrolyte additives for Li-ion batteries. *J. Power Sources* **2018**, *375*, 43−52.

https://doi.org/10.1021/acsmaterialsau.3c00010
ACS Mater. Au XXXX, XXX, XXX−XXX

(61) Ismail, I.; Noda, A.; Nishimoto, A.; Watanabe, M. XPS study of lithium surface after contact with lithium-salt doped polymer electrolytes. *Electrochim. Acta* **2001**, *46*, 1595−1603.
(62) Diao, Y.; Xie, K.; Xiong, S.; Hong, X. Insights into Li-S battery cathode capacity fading mechanisms: Irreversible oxidation of active mass during cycling. *J. Electrochem. Soc.* **2012**, *159*, A1816−A1821.
(63) Kanamura, K.; Shiraishi, S.; Takezawa, H.; Takehara, Z. XPS Analysis of the Surface of a Carbon Electrode Intercalated by Lithium Ions. *Chem. Mater.* **1997**, *9*, 1797−1804.
(64) Wood, K. N.; Teeter, G. XPS on Li-Battery-Related Compounds: Analysis of Inorganic SEI Phases and a Methodology for Charge Correction. *ACS Appl. Energy Mater.* **2018**, *1*, 4493−4504.
(65) Xu, C.; Sun, B.; Gustafsson, T.; Edström, K.; Brandell, D.; Hahlin, M. Interface layer formation in solid polymer electrolyte lithium batteries: an XPS study. *J. Mater. Chem. A* **2014**, *2*, 7256−7264.
(66) Ma, J.; Wang, C.; Wroblewski, S. Kinetic characteristics of mixed conductive electrodes for lithium-ion batteries. *J. Power Sources* **2007**, *164*, 849−856.
(67) Li, D.; Chen, L.; Wang, T.; Fan, L.-Z. 3D Fiber-Network reinforced Bicontinuous Composite Solid Electrolyte for Dendrite free Lithium Metal Batteries. *ACS Appl. Mater. Interfaces* **2018**, *10*, 7069−7078.
(68) Liu, W.; Lee, S. W.; Lin, D.; Shi, F.; Wang, S.; Sendek, A. D.; Cui, Y. Enhancing Ionic Conductivity in Composite Polymer Electrolytes with Well-aligned Ceramic Nanowires. *Nat. Energy* **2017**, *2*, 17035.
(69) Zhang, Q.; Liu, K.; Ding, F.; Li, W.; Liu, X.; Zhang, J. Safety-reinforced Succinonitrile-based Electrolyte with Interfacial Stability for High-performance Lithium Batteries. *ACS Appl. Mater. Interfaces* **2017**, *9*, 29820−29828.
(70) Yu, X.; Li, J.; Manthiram, A. Rational Design of a Laminated Dual-polymer/Polymer−Ceramic Composite Electrolyte for High-Voltage All-Solid-State Lithium Batteries. *ACS Mater. Lett.* **2020**, *2*, 317−324.

https://doi.org/10.1021/acsmaterialsau.3c00010
ACS Mater. Au XXXX, XXX, XXX−XXX